ADVANCED MATERIALS INTERFACES
Open Access
www.advmatinterfaces.de

Probing of Polarization Reversal in Ferroelectric (Al,Sc)N Films Using Single- and Tri-Layered Structures With Different Sc/(Al+Sc) Ratio

*Shinnosuke Yasuoka, Takao Shimizu, Kazuki Okamoto, Nana Sun, Soshun Doko, Naoko Matsui, Toshikazu Irisawa, Koji Tsunekawa, Alexei Gruverman, and Hiroshi Funakubo**

Wurtzite-(Al,Sc)N films are promising candidates for ferroelectric memory devices owing to their outstanding properties. However, there are many challenges on the way to practical applications, including lowering an electric field required for polarization switching. Understanding the switching kinetics, especially the starting point of polarization reversal, is key to designing materials with desired properties. Here, the impact of Sc concentration and segregation on the switching kinetics for (Al,Sc)N capacitors is investigated by evaluating time- and field-dependences of the switching polarization for the tri-layered (Al,Sc)N films with various Sc/(Al+Sc) ratios. The remanent polarization of stacked films slightly decreased compared to those of the single-layered films with the same average Sc/(Al+Sc) ratio, while their coercive fields depended on the average Sc content in (Al,Sc)N. The ferroelectric switching behavior suggests the possibility of nucleation originating from the Sc-rich region and the sequential switching mechanism for individual layers, which is unique to multilayered films. This shows a possibility that nucleations of the polarization switching start not from the interface between the (Al,Sc)N films and the electrodes. The unique switching kinetics in tri-layered (Al,Sc)N films have provided new insights into the field of ferroelectric switching in wurtzite-nitrides.

1. Introduction

Ferroelectric polarization switching is the transition between two stable states of spontaneous polarization induced by an external electric field. Due to the polarization nonvolatility, materials possessing such capability can be used in low-energy and high-density integrated memory devices, such as ferroelectric random-access memory (FeRAM) and ferroelectric tunnel junction (FTJ).[1–3] Moreover, the multifunctionality of ferroelectrics is also promising for novel applications in other areas, including negative capacitance and neuromorphic computing.[4,5] However, the development of the next-generation ferroelectric-based devices requires overcoming multiple challenges related to the enhancement of performance and reliability.

In contrast to conventional perovskite ferroelectrics, HfO_2-based films are CMOS-compatible and exhibit robust polarization at the nanoscale thickness.[6–8] Polarization switching in hexagonal wurtzite-structured nitride was experimentally demonstrated in (Al,Sc)N film by Fichtner et al.[9] The AlN-based materials, which are already widely used in piezoelectric devices, provide significant advantages from a practical perspective because they can be fabricated at room temperature and possess good ferroelectric properties in films on Si substrate.[10,11] Not only B- and Y-doped AlN films but even GaN-based films have been

S. Yasuoka, K. Okamoto, N. Sun, H. Funakubo
Department of Materials Science and Engineering
Tokyo Institute of Technology
Yokohama 226-8502, Japan
E-mail: funakubo.h.aa@m.titech.ac.jp

The ORCID identification number(s) for the author(s) of this article can be found under https://doi.org/10.1002/admi.202400627

DOI: 10.1002/admi.202400627

T. Shimizu
Research Center for Functional Materials
National Institute for Materials Science
Tsukuba 305-0044, Japan

T. Shimizu
PRESTO
Japan Science and Technology Agency
4-1-8 Honcho, Kawaguchi-shi, Saitama 332-0012, Japan

S. Doko, N. Matsui, T. Irisawa, K. Tsunekawa
Canon ANELVA Corporation
5-1 Kurigi 2-chome, Asao-ku, Kawasaki-shi, Kanagawa 215-8550, Japan

A. Gruverman
Department of Physics and Astronomy
University of Nebraska
Lincoln, NE 68588-0299, USA

reported to exhibit ferroelectricity.[12–15] The ferroelectric properties of wurtzite-structured nitrides are strongly influenced by the dopant elements, especially the remanent polarization (P_r) and coercive field (E_c) of the (Al,Sc)N films, which decrease with increasing the Sc/(Al+Sc)N ratio in the film.[9,16] This is due to the change in the coordination environment of the cations from four-coordinated tetrahedrons to five-coordinated bipyramids that describe the metastable layered hexagonal structure of ScN, resulting in a flattening of the energy landscape.[17,18] Although it was shown that the P_r and E_c values of (Al,Sc)N films can be controlled by strain-tunable crystal anisotropy, the ferroelectric properties of AlN- and GaN-based films are mainly dominated by the level of Sc dopants.[10,19,20]

Recently, we have reported the temperature- and frequency-dependent switching kinetics in the $(Al_{0.8}Sc_{0.2})N$ capacitors, which follow the invariant polarization switching model and domain-wall motion regime even at high temperatures and frequencies.[21] The switching behavior of the (Al,Sc)N films can be fitted by the Kolmogorov-Avrami-Ishibashi (KAI) model described by the following equation:

$$\Delta P = 1 - exp\left[-\left(\frac{t}{t_0}\right)^n\right] \quad (1)$$

where t_0 and n are the characteristics switching time and dimension of the domain growth, respectively.[22] Yazawa et al. reported a composite extended KAI model, where the nucleation rate peaks after the growth of switched nuclei.[23] Furthermore, it has been reported that the investigations of the switching mechanisms, such as observation of polarization switching at the atomic level and prediction of the switching pathway in addition to the switching kinetics.[24] In general, ferroelectric polarization switching is expected to occur from inverse domain nuclei generated around the electrode interface.[25] On the other hand, modeling using density functional theory (DFT) based quantum molecular dynamics (QMD) predicted that inhomogeneous Sc distribution reduces the activation barrier.[26] These calculations imply that the insertion of layers with small E_c at the electrode interfaces may lead to the reduction of the intrinsically large E_c of the (Al,Sc)N systems. Up to now, there are no studies that have investigated the polarization reversal in (Al,Sc)N structures composed of stacked layers with different coercive fields. In addition, the impact of doping level on the switching kinetics in the (Al,Sc)N films has not been well understood.

In this study, we investigated the ferroelectric switching kinetics of the single- and tri-layered (Al,Sc)N structures with various Sc/(Al+Sc)N ratios observing changes in the ferroelectric properties and the dimensions of the growing domains.

2. Results and Discussion

2.1. Crystal Structure

Single-layered films of the 150-nm-thick $(Al_{0.9}Sc_{0.1})N$ (pure Sc10%) and $(Al_{0.7}Sc_{0.3})N$ (pure Sc30%) and tri-layered films of [10-nm-thick $(Al_{0.7}Sc_{0.3})N$]/[130-nm-thick $(Al_{0.9}Sc_{0.1})N$]/[10-nm-thick $(Al_{0.7}Sc_{0.3})N$] (Sc30/10/30%) [10-nm-thick $(Al_{0.9}Sc_{0.1})N$]/[130-nm-thick $(Al_{0.7}Sc_{0.3})N$]/[10-nm-thick $(Al_{0.9}Sc_{0.1})N$] (Sc10/30/10%) were deposited on a (111)Pt/TiO_x/SiO_2/Si substrates as shown in **Figure 1**. Here, the average Sc/(Al+Sc) ratio of Sc30/10/30% and Sc10/30/10% films were ≈13% and 27%, respectively. The microstructure of Sc30/10/30% film is shown in Figure S1 (Supporting Information). It can be seen that the grain is connected in the tri-layer and extends continuously from one electrode to the other. We expect there might be no obvious change in the grain or crystallite size in the tri-layer stack compared to the single-layer structure.

Figure 2a,b show the out-of-plane XRD and in-plane GIXRD patterns of the (Al,Sc)N films, respectively. Based on the standard powder diffraction patterns of wurtzite AlN (PDF#00-025-1133), the films did not show any other secondary phases. Only *00l* and *h00*/*hk0* diffraction peaks were observed in the out-of-plane XRD and in-plane GIXRD patterns, respectively, excluding those coming from the electrode and substrate. These results indicate that all samples including stacked films consisted of a (001)-out-of-plane-oriented wurtzite structure phase. It should be noted that the peaks from the single-layered films (Sc10% and Sc30% films) in the in-plane XRD patterns were almost symmetrical, whereas the coexistence of two peaks was observed for the tri-layered films (Sc30/10/30% and Sc10/30/10% films). This suggests that the compositional diffusion has occurred within the stacked films, which is also ascertained by RBS measurements (See Figure S2, Supporting Information). We attempted to separate peaks in order to investigate the influence of the strain. **Figure 3**a,b shows the enlarged *110* diffraction peaks of Sc30/10/30% and Sc10/30/10% films. The asymmetric peaks derived from (Al,Sc)N with different Sc/(Al+Sc) ratios were separated by fitting with a Pearson VII based on the peak positions of the single-layered films.[27] The difference in peak intensities may contribute to the intensities derived from the respective layers with different Sc content ratios as well as the film thickness, considering the decrease in peak intensity with increasing Sc/(Al+Sc) ratio of (Al,Sc)N films.[28] Figure 3c shows the in-plane *a*-axis lattice constant with error bars as a function of the average Sc/(Al+Sc) ratio of the entire film. This *a*-axis lattice constant was derived from the deconvoluted fits of Figure 3a,b. Based on the in-plane lattice parameters of pure Sc10% and 30% films, it was found that the middle layers, which constitute the majority of the stacked films, were not significantly affected. In contrast, the minority top and bottom layers were strained by the stresses applied from the middle layers and/or bottom electrodes. Here, the *a*-axis lattice constant of Sc10% layers in the Sc10/30/10% film increased relative to that of the pure Sc10% film, suggesting that the top layer contributes more than the bottom layer to the change in the lattice constant of the covering layer because the lower layer on Pt is expected to be under compressive stress.[29] Even taking into account the stress-based lattice changes at this interface, the inserted layers with different Sc/(Al+Sc) ratios are likely to influence the enhancement of nucleation at the electrode interface because the E_c of each layer is different.

2.2. Ferroelectric Properties

As the next step, the ferroelectric properties were investigated for the four films shown in Figure 1. **Figure 4**a shows the electric

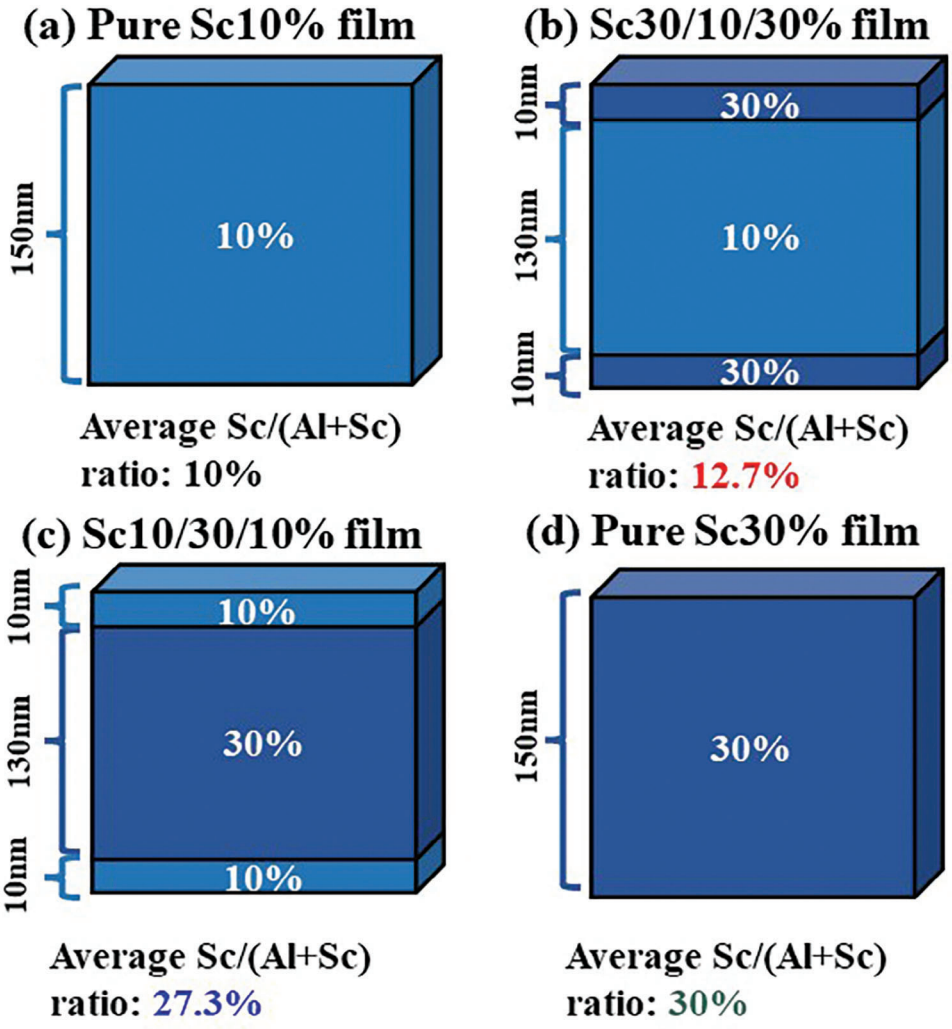

Figure 1. Schematic illustrations of a) the 150-nm-thick $(Al_{0.9}Sc_{0.1})N$ (pure Sc10%), b) 10-nm-thick $(Al_{0.7}Sc_{0.3})N$/130-nm-thick $(Al_{0.9}Sc_{0.1})N$/10-nm-thick $(Al_{0.7}Sc_{0.3})N$ (Sc30/10/30%), c) 10-nm-thick $(Al_{0.9}Sc_{0.1})N$/130-nm-thick $(Al_{0.7}Sc_{0.3})N$/10-nm-thick $(Al_{0.9}Sc_{0.1})N$ (Sc10/30/10%), and d) 150-nm-thick $(Al_{0.7}Sc_{0.3})N$ (pure Sc30%).

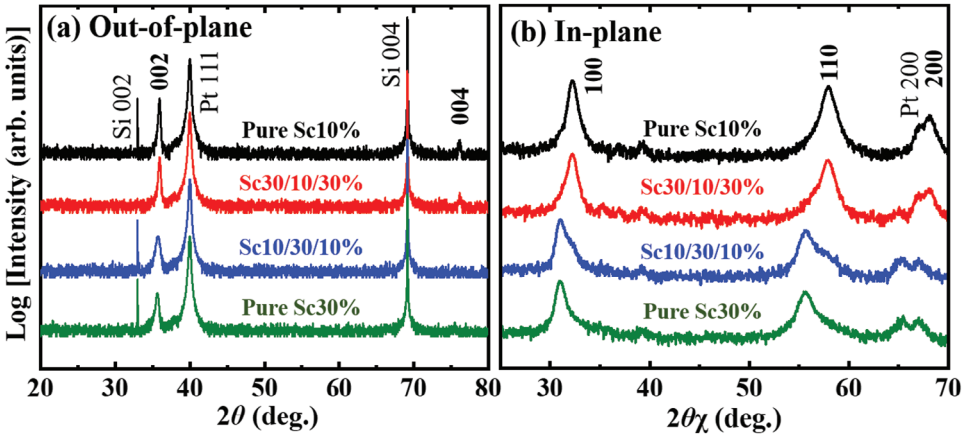

Figure 2. a) Out-of-plane XRD and b) in-plane GIXRD patterns for (Al,Sc)N films with various Sc/(Al+Sc) ratios.

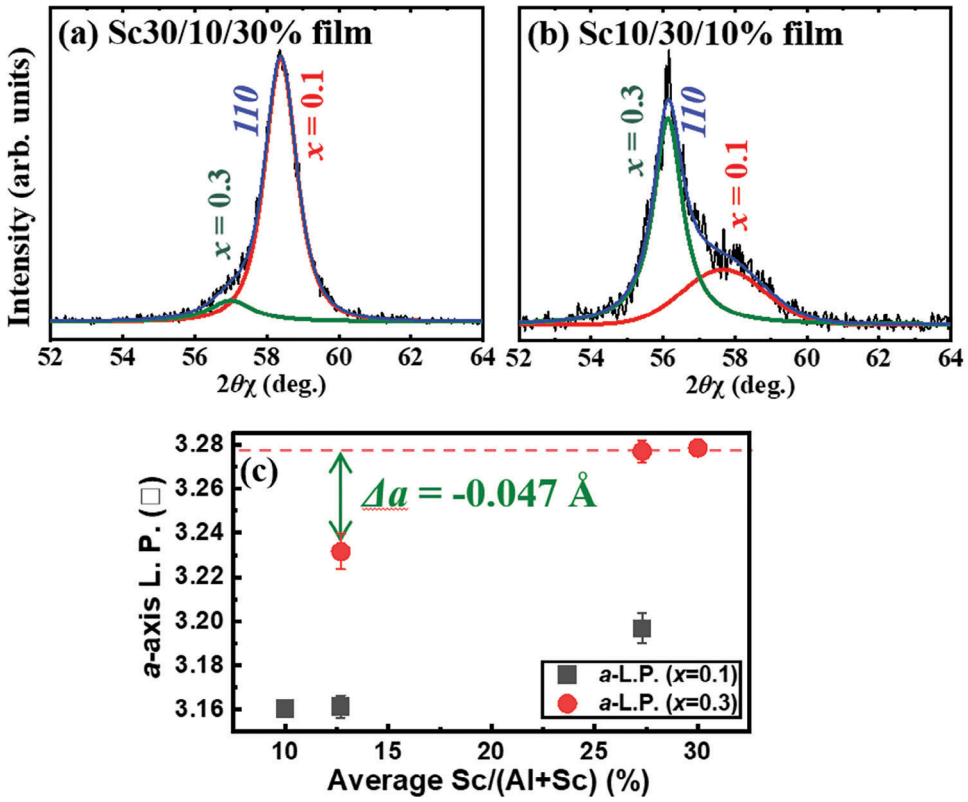

Figure 3. Enlarged views ≈*110* diffraction peaks including the results in peak fitting based on the peak position of the pure Sc content films in the a) Sc30/10/30% and b) Sc10/30/10% films. c) Average Sc/(Al+Sc) ratio dependences of strain for single- and tri-layered (Al,Sc)N films.

field dependency of the switched polarization values for the reversal from the upward to downward polarization obtained by the PUND method. The pulse and interval widths of 10 µs and 50 µs were used in the PUND measurement, as shown in the inset. In the PUND measurements, although a perfect saturation behavior is absent, a saturation trend can be found for all samples including the stacked films. This deviation from saturation can be partially attributed to the enhanced leakage current under high electric fields.[30] The breakdown field change in (Al,Sc)N films with various average Sc/(Al+Sc) ratios was shown in Figure S3 (Supporting Information). It can be seen that the E_{BD} of Sc30/10/30% film was on the line of the average composition dependency of E_{BD} as shown in the solid line. While Sc10/30/10% film increased slightly against the trend. This increase is in good agreement with the result of the multilayered architecture of (Al,Sc)N films reported by Zheng et al.[31]

The relative dielectric constant of these films as a function of the average Sc/(Al+Sc) ratio is shown in Figure S4 (Supporting Information). The relative dielectric constant of the pure 30% film is slightly larger than that of the pure 10% film, which is in good agreement with our previous work.[29] The relative dielectric constant of tri-layers is between the values of pure 10% and 30% films, because of the sandwiched layers with different compositions. Figure 4b shows the $2P_r$ and E_c as a function of the average Sc/(Al+Sc) ratios in the entire (Al,Sc)N films. The $2P_r$ of the stacked films slightly decreased in comparison to the expected values based on the average composition of entire films. On the other hand, their E_c almost continuously depended on the average Sc/(Al+Sc) ratios for entire average (Al,Sc)N films as shown in Figure 4b, indicating that the impact of the stacking layer on E_c is not so obvious. The slight decreases in $2P_r$ values of the stacked films are presumably due to charge compensation between layers of different compositions or the stress from the upper and lower layer on Pt as shown in the XRD results. Within a certain voltage range, the $2P_r$ values of the Sc30/10/30% and Sc10/30/10% films are higher than those of the pure Sc30% and Sc10% films. The dependence of E_c on the average composition in the entire film suggests that the insertion of a low-E_c layer at the film-electrode interface, which is generally expected to promote nucleation, has no large effect on decreasing the net E_c of the entire stacked structure. Furthermore, these results imply that the nucleation sites that control the E_c may be at the Sc-rich regions of the film, not at the interface because the generation of the nuclei in the low-E_c layer does not significantly contribute to the acceleration of polarization switching of the capacitor structures. This assumption is supported by the model based on theoretical calculations suggesting that polarization switching occurs at the Sc-rich region[26] and the domain nucleation energy is higher than that of domain growth.[32] Experimentally, the in situ scanning transmission electron microscopy (STEM) observations have confirmed that nucleation occurs in the regions where the largest local electric field is applied.[24] Moreover, E_c as a function of Sc content is almost on the same line for Sc-AlN and Sc-GaN.[20] The additional experiment of examining different stack orders with the same % combinations will be conducted in the next step work.

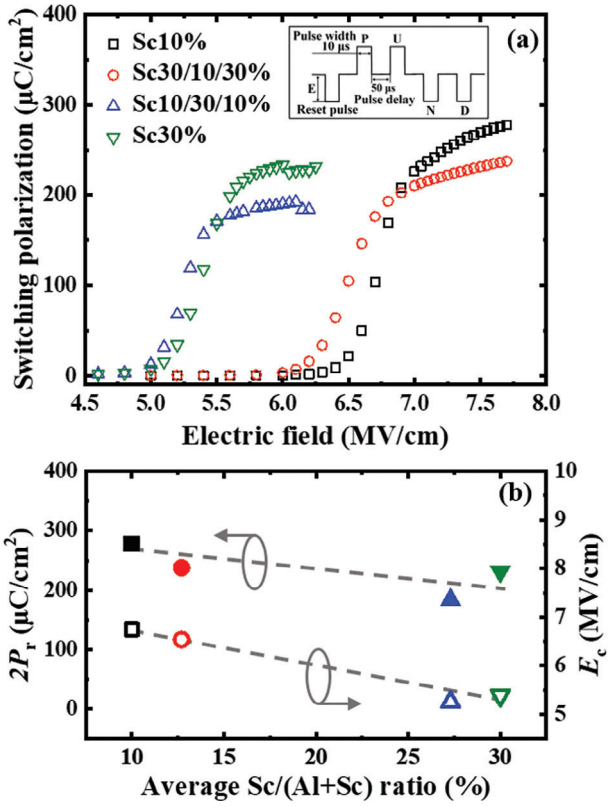

Figure 4. a) Switching polarization values obtained by PUND in the (Al,Sc)N films with various Sc/(Al+Sc) ratios as a function of the electric field. b) Average Sc/(Al+Sc) ration dependences of $2P_r$ and E_c estimated from (a).

2.3. Switching Kinetics

Figure 5a shows the electric field dependence of the current–time (I–t) curves obtained from the PUND measurements of the Sc10% film. The peak representing the ferroelectric switching current exhibits a sharp shape as the applied electric field increases, indicating a high-speed polarization switching. The polarization switching time (t_{sw}) was defined as the time it takes for polarization switching to be completed.[25] Figure 5b shows the t_{sw} estimated from the I–t curves of each film as a function of the electric field normalized by E_c along with the previously reported data for $(Hf,Ce)O_2$, $Pb(Zr_{0.52}Ti_{0.48})O_3$, and $LiNbO_3$.[33–35] The normalized electric field dependencies of t_{sw} are almost the same regardless of film stacking, suggesting that the Sc concentration and the stack structure had no significant contribution to the growth speed of the switching domain. The switching of the (Al,Sc)N capacitors for the applied electric fields normalized to the respective E_c is faster than of the ferroelectrics with different structures. The relatively high linearity of (Al,Sc)N film allows us to expect fast polarization switching at larger E because the dominant mode of switching remains unchanged, as shown by the dashed line in Figure 5b. Merz's law is an empirical model describing the relationship between t_{sw} and E as follows:

$$t_{sw} = t_0 \exp\left(\frac{E_a}{E}\right) \quad (2)$$

where t_0 and E_a are the theoretical switching times for an infinitely strong electric field and the activation field, respectively. It can be seen that E_a for (Al,Sc)N, which exhibits a similar E_c trend with respect to Sc/(Al+Sc) ratio, is significantly larger than those of other ferroelectric materials (Figure 5c). The activation energy is the smallest in the tri-layer Sc10/30/10% film, due to the well crystalline quality by inserting a pure 10% layer. Because the lattice constant of pure 10% film is close to the lattice constant of the underlying Pt bottom electrode, results in a small lattice mismatch. Landau–Devonshire thermodynamic modeling was introduced for the phenomenological description of the relationship between the Gibbs free energy and polarization as shown in Figure 5d. This well depth corresponds to the switching barrier height which relates to the intrinsic ferroelectric coercive field.[36] Based on the reported DFT calculation results, the polarization dependence of the switching barrier was plotted.[37] It can be seen that the increased Sc composition reduced the energy barrier for the switching, which is in good agreement with the reduced E_a with high Sc composition. The sharp slop of the switching barrier corresponds to the fast-switching speed of the domain. It can be seen that (Al,Sc)N film shows a faster switching speed and higher material-specific deep energy landscape compared to those of the traditional ferroelectric materials, unlike E_c, which is generally promoted by the effects of interfaces and defects.

To reveal the effect of the Sc concentration and the stacking structure of the switching mechanism, we investigated the field dependencies of the switching kinetics. **Figure** 6a–d shows the switched polarization fraction as a function of time for the different electric fields for pure Sc10%, Sc30/10/30%, Sc10/30/10%, and pure Sc30% films, respectively. The switching pulse and interval widths of 0.5–1000 μs and 2.5–5000 μs were shown in the inset. The dashed lines correspond to the KAI fitting using Equation (1). These results indicate that not only the polarization switching occurs in a wide range of electric fields and time scales, but also that the switching behavior of the single-layered films is well-fitted by the KAI model while there is a slight deviation from this model in the multilayered films. Figure 6e,f show the field and the average Sc/(Al+Sc) ratio dependences of the n values obtained from the KAI fitting, respectively. The n values in the pure Sc10% and Sc30% films are ≈2, increasing slightly with an increase in the field, which is also in agreement with the 3D domain growth reported by Calderon et al.[24] It indicates the 2D in-plane propagation of the switched domains is a rate determination step for the pure films.[23] On the other hand, the n values of the stacked films are almost 1 regardless of the electric field, indicating the rate determination step of the 1D out-of-plane propagation of the switched domains. It is possible that the mechanism of polarization switching in (Al,Sc)N multilayered films cannot be explained by the KAI model. Figure S5a,b (Supporting Information) show the time dependence of $\Delta P/P_{max}$ alongside the results of nucleation-limited-switching (NLS) fitting and a Lorentzian distribution function that describes the dispersion of t_0 in individual domains for the Sc30/10/30% films. The figures indicate that our data can also be well-fitted to the NLS model. However, the full width at half maximum of the distribution function shows no obvious change with respect to the applied E. The full width at half maximum previously reported for ferroelectric materials fitted to the NLS model exhibits a marked dependence on E.[38]

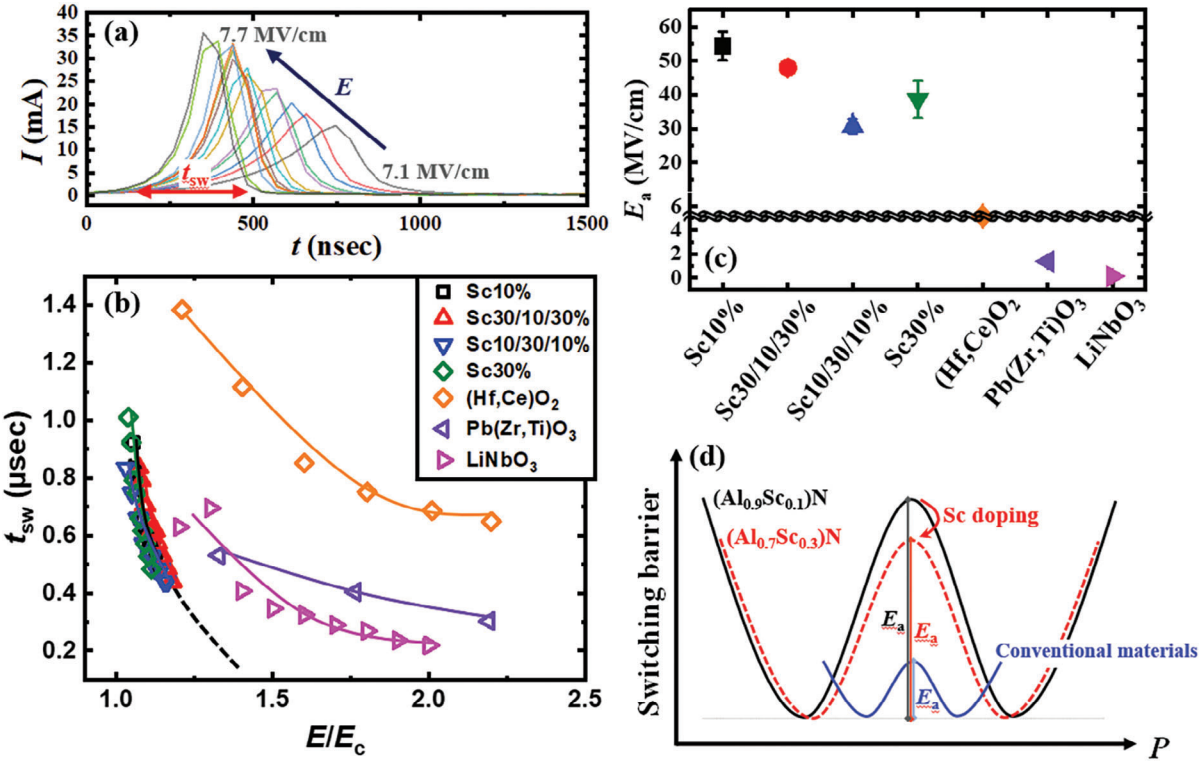

Figure 5. a) Electric field dependency of the switching current-time curves in $(Al_{0.9}Sc_{0.1})N$ film. b) t_{sw} as a function of E normalized by E_c and c) E_a in (Al,Sc)N films, together with the reported data for $(Hf,Ce)O_2$,[33] $Pb(Zr,Ti)O_3$,[34] and $LiNbO_3$.[35] d) Schematic illustrations of the switching barrier for (Al,Sc)N.

Therefore, the results suggest that the KAI model is sufficient to understand the switching kinetics of wurtzite-type $(Al_{0.8}Sc_{0.2})N$ films in this work.

Based on the data in Figure 4, these results imply that the nucleation sites that control the E_c may be at the Sc-rich regions of the film, not at the interface because the generation of the nuclei in the low-E_c layer does not significantly contribute to the acceleration of polarization switching of the capacitor structures. This assumption is supported by the model based on theoretical calculations suggesting that polarization switching occurs at the Sc-rich region[26] and the domain nucleation energy is higher than that of domain growth.[32] Experimentally, the in situ scanning transmission electron microscopy (STEM) observations have confirmed that nucleation occurs in the regions where the largest local electric field is applied.[24] Moreover, E_c as a function of Sc content isis almost on the same line for Sc-AlN and Sc-GaN.[20] In addition, the n values of ≈1 followed the 1D out-of-plane propagation of the switched domains. And normalized electric field dependencies of t_{sw} are almost the same regardless of film stacking, suggesting that the Sc concentration and the stack structure had no significant contribution to the growth speed of the switching domain. Following the assumption that the nuclei are not generated at the film-electrode interface, the switching mechanism in the multilayered films can be attributed to the pseudo 1D growth via a two-step switching process: i) subsequent switching in the Sc-poor layers with high E_c; ii) polarization switching complete of the entire film, as schematically shown in Figure 6g. The net polarization switching caused by kinetics in each layer supports the invariance of E_c in the multilayered films shown in Figure 4b. Thus, investigation of the switching kinetics in single- and tri-layered films has provided new insights into the field of ferroelectric switching in wurtzite-structured (Al,Sc)N capacitors.

3. Conclusion

The switching kinetics in the single- and tri-layered (Al,Sc)N films with various Sc/(Al+Sc) ratios were investigated. Their ferroelectric properties and switching rates were evaluated by PUND measurements. The ferroelectric switching behaviors of (Al,Sc)N structures composed of several layers suggest a possibility of nucleation originating in the Sc-rich regions in a switching mechanism unique to the stacked films. These results provide a critical step for understanding the switching kinetics of the wurtzite-structured ferroelectric nitrides.

4. Experimental Section

All films shown in Figure 1 were deposited on (111)$Pt/TiO_x/SiO_2/Si$ substrates via the dual source reactive sputtering method using Al (99.999%) and Sc (99.99%) metal targets. The Sc/(Al+Sc) ratio and film thickness were controlled by RF powers and deposition time, respectively, and determined by Rutherford backscattering spectrometry (RBS) (HRBS-V500, KOBELCO) and wavelength-dispersive X-ray fluorescence spectrometry (XRF) (PW4400, PANalytical). The results of RBS analysis indicate the fabricated stacked (Al,Sc)N structures as shown in Figure S2 (Supporting Information)

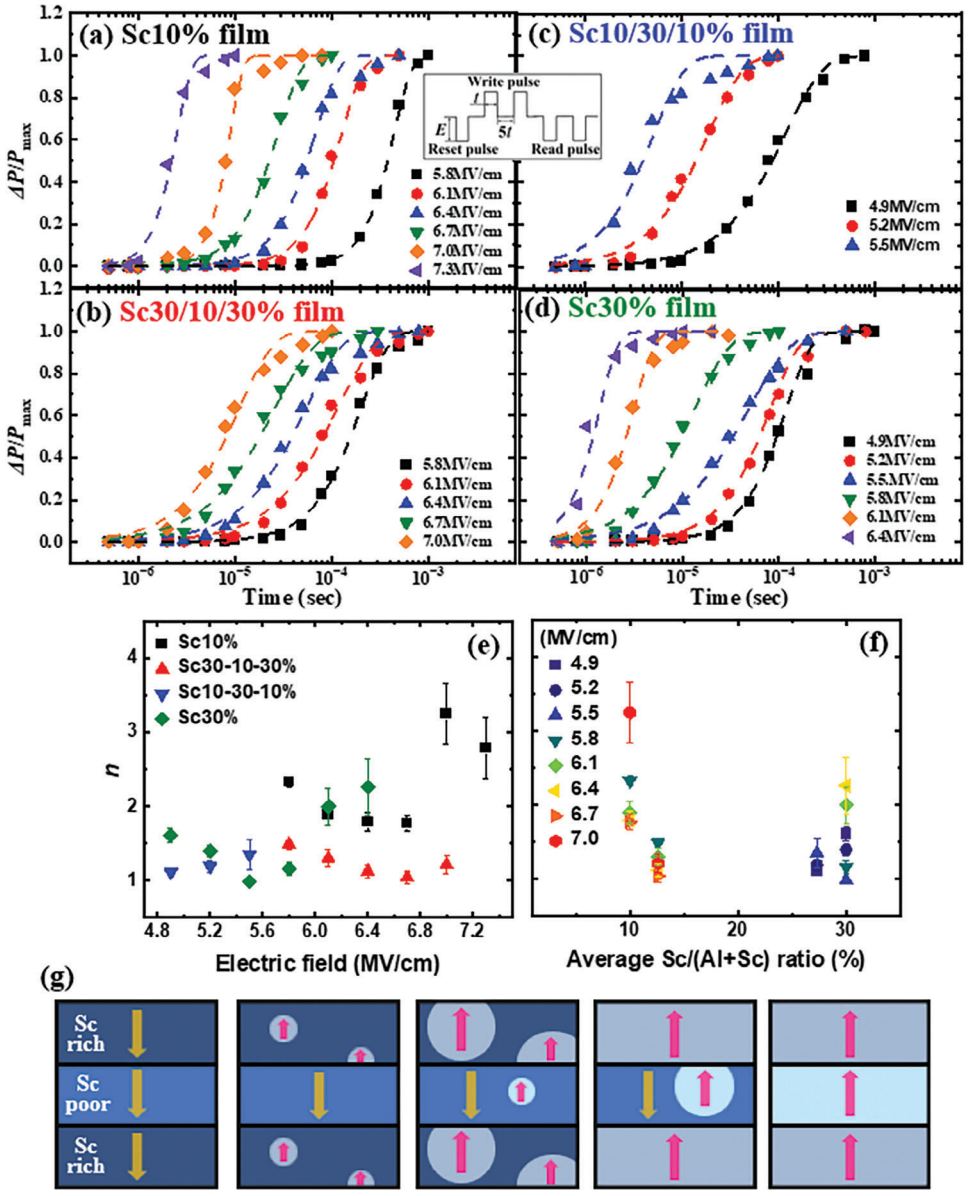

Figure 6. Electric field dependences of the fraction of the switching polarization as a function of time in the a) pure Sc10%, b) Sc30/10/30%, c) Sc10/30/10%, and d) pure Sc30% films. e) Electric field and f) average Sc/(Al+Sc) ratio dependences of *n* values obtained from (a–d). g) Schematic illustrations of the polarization switching process by applying an electric field.

of the supplementary material. The details of the sputtering condition of (Al,Sc)N were described elsewhere.[16]

The crystal structure was characterized by out-of-plane and in-plane measurements in XRD (X'Pert-MRD, Philips) and grazing-incident XRD (GIXRD) (Smart Lab, Rigaku), respectively. 100-nm-thick Pt top-electrodes of 50 and 100 μm in diameter were fabricated via electron beam evaporation through a shadow mask at room temperature. The ferroelectric properties and switching kinetics of Pt/(Al,Sc)N/Pt capacitors were evaluated by measuring the switched polarization as a function of the applied electric field and time. To determine the correct P_r and E_c values that eliminate the leakage current contribution, the positive-up-negative-down (PUND) measurements were carried using a pulse and interval width of 10 μs and 50 μs. In PUND measurements, the $2P_r$ was defined as the value 1.1 times the inflection point at which the switching polarization value begins to saturate, while E_c was defined as the electric field at which the net polarization was zero.

Supporting Information

Supporting Information is available from the Wiley Online Library or from the author.

Acknowledgements

This work was partly supported by the project "Element Strategy Initiative to Form a Core Research Center (JPMXP0112101001)" of MEXT,

MEXT Initiative to Establish Next-generation Novel Integrated Circuits Centers (X-NICS) (JPJ011438), MEXT Program: Data Creation and Utilization Type Material Research and Development Project (Grant Number: JPMXP1122683430). This work was also partly supported by the Japan Society for the Promotion of Science (JSPS) KAKENHI (Grant No. 21H01617, 22K18307, and 22K20427) and by JST PRESTO (Grant Number: JPMJPR20B3), JST ASPIRE (Grant Number: JPMJAP2312), Japan. Support of the TIT World Research Hub program is gratefully acknowledged.

Conflict of Interest

The authors declare no conflict of interest.

Data Availability Statement

The data that support the findings of this study are available from the corresponding author upon reasonable request.

Keywords

(Al,Sc)N films, multiple layers, Sc concentration, switching kinetics

Received: July 26, 2024
Revised: September 9, 2024
Published online: October 13, 2024

[1] J. F. Scott, C. A. Paz De Araujo, *Science* **1989**, *246*, 1400.
[2] D. J. Kim, H. Lu, S. Ryu, C. W. Bark, C. B. Eom, E. Y. Tsymbal, A. Gruverman, *Nano Lett.* **2012**, *12*, 5697.
[3] K. H. Kim, I. Karpov, R. H. Olsson, D. Jariwala, *Nat. Nanotechnol.* **2023**, *18*, 422.
[4] A. I. Khan, K. Chatterjee, B. Wang, S. Drapcho, L. You, C. Serrao, S. R. Bakaul, R. Ramesh, S. Salahuddin, *Nat. Mater.* **2015**, *14*, 182.
[5] J. Li, C. Ge, J. Du, C. Wang, G. Yang, K. Jin, *Adv. Mater.* **2020**, *32*, 1905764.
[6] K. Uchino, E. Sadanaga, T. Hirose, *J. Am. Ceram. Soc.* **1989**, *72*, 1555.
[7] P. Gao, Z. Zhang, M. Li, R. Ishikawa, B. Feng, H. Liu, Y. Huang, N. Shibata, X. Ma, S. Chen, J. Zhang, K. Liu, E. Wang, D. Yu, *Nat. Commun.* **2017**, *8*, 15549.
[8] T. Mimura, T. Shimizu, H. Uchida, O. Sakata, H. Funakubo, *Appl. Phys. Lett.* **2018**, *113*, 102901.
[9] S. Fichtner, N. Wolff, F. Lofink, L. Kienle, B. Wagner, *J. Appl. Phys.* **2019**, *125*, 114103.
[10] S. Yasuoka, T. Shimizu, A. Tateyama, M. Uehara, H. Yamada, M. Akiyama, H. Funakubo, *Phys. Status Solidi Appl. Mater. Sci.* **2021**, 2100302.
[11] Sung-Lin Tsai, T. Hoshii, H. Wakabayashi, K. Tsutsui, T-K. Chung, E. Y. Chang, K. Kakushima, *Appl. Phys. Lett.* **2021**, *118*, 082902.
[12] J. Hayden, M. D. Hossain, Y. Xiong, K. Ferri, W. Zhu, M. V. Imperatore, N. Giebink, S. Trolier-Mckinstry, I. Dabo, J. P. Maria, *Phys. Rev. Mater.* **2021**, *5*, 044412.
[13] D. Wang, S. Mondal, J. Liu, M. Hu, P. Wang, S. Yang, D. Wang, Y. Xiao, Y. Wu, T. Ma, Z. Mi, *Appl. Phys. Lett.* **2023**, *123*, 033504.
[14] D. Wang, P. Wang, B. Wang, Z. Mi, *Appl. Phys. Lett.* **2021**, *119*, 111902.
[15] M. Uehara, R. Mizutani, S. Yasuoka, T. Shiraishi, T. Shimizu, H. Yamada, M. Akiyama, H. Funakubo, *Appl. Phys. Lett.* **2021**, *119*, 172901.
[16] S. Yasuoka, T. Shimizu, A. Tateyama, M. Uehara, H. Yamada, M. Akiyama, Y. Hiranaga, Y. Cho, H. Funakubo, *J. Appl. Phys. 128*, 114103.
[17] F. Tasnádi, B. Alling, C. Höglund, G. Wingqvist, J. Birch, L. Hultman, I. A. Abrikosov, *Phys. Rev. Lett.* **2010**, *104*, 137601.
[18] S. Zhang, D. Holec, W. Y. Fu, C. J. Humphreys, M. A. Moram, *J. Appl. Phys.* **2013**, *114*, 133510.
[19] S. Yasuoka, R. Mizutani, R. Ota, T. Shiraishi, T. Shimizu, M. Uehara, H. Yamada, M. Akiyama, H. Funakubo, *ACS Appl. Electron. Mater.* **2022**, *4*, 5165.
[20] M. Uehara, R. Mizutani, S. Yasuoka, T. Shimizu, H. Yamada, M. Akiyama, H. Funakubo, *Appl. Phys. Express* **2022**, *15*, 081003.
[21] S. Yasuoka, R. Mizutani, R. Ota, T. Shiraishi, T. Shimizu, K. Okamoto, M. Uehara, H. Yamada, M. Akiyama, H. Funakubo, *Appl. Phys. Lett.* **2023**, *123*, 202902.
[22] Y. Ishibashi, Y. Takagi, *J. Phys. Soc. Japan* **1971**, *31*, 506.
[23] K. Yazawa, J. Hayden, J. Maria, W. Zhu, S. Trolier-mckinstry, G. L. Brennecka, *Mater. Horiz.* **2023**, *10*, 2936.
[24] S. C. V., J. Hayden, S. M. Baksa, W. Tzou, S. Trolier-mckinstry, I. Dabo, J. Maria, E. C. Dickey, *Science* **2023**, *380*, 1034.
[25] W. J. Merz, *Phys. Rev.* **1954**, *95*, 690.
[26] A. Krishnamoorthy, S. C. Tiwari, A. Nakano, *Nanotechnology* **2021**, *32*, 49LT02.
[27] H. Wang, J. Zhou, *J. Appl. Cryst.* **2005**, *38*, 830.
[28] M. Akiyama, T. Kamohara, K. Kano, A. Teshigahara, Y. Takeuchi, N. Kawahara, *Adv. Mater.* **2009**, *21*, 593.
[29] S. Yasuoka, R. Mizutani, R. Ota, T. Shiraishi, T. Shimizu, S. Yasui, Y. Ehara, K. Nishida, M. Uehara, H. Yamada, M. Akiyama, Y. Imai, O. Sakata, H. Funakubo, *J. Ceram. Soc. Japan* **2022**, *130*, 436.
[30] D. Wang, P. Wang, S. Mondal, J. Liu, M. Hu, M. He, S. Nam, W. Peng, S. Yang, D. Wang, Y. Xiao, Y. Wu, A. Mortazawi, Z. Mia, *Appl. Phys. Lett.* **2023**, *123*, 103506.
[31] J. X. Zheng, D. Wang, P. Musavigharavi, M. M. A. Fiagbenu, D. Jariwala, E. A. Stach, R. H. Olsson, *J. Appl. Phys.* **2021**, *130*, 144101.
[32] Y. H. Shin, I. Grinberg, I. W. Chen, *Nature* **2007**, *449*, 881.
[33] F. Cüppers, K. Hirai, H. Funakubo, *Nano Converg* **2022**, *9*, 56.
[34] E. Tokumitsu, N. Tanisake, H. Ishiwara, *Jpn. J. Appl. Phys.* **1994**, *33*, 5201.
[35] J. Jiang, X. J. Meng, D. Q. Geng, A. Q. Jiang, *J. Appl. Phys.* **2015**, *117*, 104101.
[36] K. Yazawa, A. Zakutayev, G. L. Brennecka, *Appl. Phys. Lett.* **2022**, *121*, 042902.
[37] H. Wang, N. Adamski, S. Mu, C. G. Walle, *J. Appl. Phys.* **2021**, *130*, 104101.
[38] A. K. Tagantsev, I. Stolichnov, N. Setter, J. S. Cross, M. Tsukada, *Phys. Rev. B.* **2002**, *66*, 214109.